Calcified Tissue International (2024) 114:171–181
https://doi.org/10.1007/s00223-023-01158-0

ORIGINAL RESEARCH

An Additional *Lrp4* High Bone Mass Mutation Mitigates the *Sost*-Knockout Phenotype in Mice by Increasing Bone Remodeling

Gretl Hendrickx[1,2] · Eveline Boudin[1] · Ligia Mateiu[1] · Timur A. Yorgan[3] · Ellen Steenackers[1] · Michaela Kneissel[4] · Ina Kramer[4] · Geert Mortier[1,2] · Thorsten Schinke[3] · Wim Van Hul[1]

Received: 10 July 2023 / Accepted: 31 October 2023 / Published online: 5 December 2023

Abstract

Pathogenic variants disrupting the binding between sclerostin (encoded by *SOST*) and its receptor LRP4 have previously been described to cause sclerosteosis, a rare high bone mass disorder. The sclerostin-LRP4 complex inhibits canonical WNT signaling, a key pathway regulating osteoblastic bone formation and a promising therapeutic target for common bone disorders, such as osteoporosis. In the current study, we crossed mice deficient for *Sost* ($Sost^{-/-}$) with our p.Arg1170Gln *Lrp4* knock-in ($Lrp4^{KI/KI}$) mouse model to create double mutant $Sost^{-/-}$;$Lrp4^{KI/KI}$ mice. We compared the phenotype of $Sost^{-/-}$ mice with that of $Sost^{-/-}$;$Lrp4^{KI/KI}$ mice, to investigate a possible synergistic effect of the disease-causing p.Arg1170Trp variant in *Lrp4* on *Sost* deficiency. Interestingly, presence of $Lrp4^{KI}$ alleles partially mitigated the $Sost^{-/-}$ phenotype. Cellular and dynamic histomorphometry did not reveal mechanistic insights into the observed phenotypic differences. We therefore determined the molecular effect of the $Lrp4^{KI}$ allele by performing bulk RNA sequencing on $Lrp4^{KI/KI}$ primary osteoblasts. Unexpectedly, mostly genes related to bone resorption or remodeling (*Acp5*, *Rankl*, *Mmp9*) were upregulated in $Lrp4^{KI/KI}$ primary osteoblasts. Verification of these markers in $Lrp4^{KI/KI}$, $Sost^{-/-}$ and $Sost^{-/-}$;$Lrp4^{KI/KI}$ mice revealed that sclerostin deficiency counteracts this $Lrp4^{KI/KI}$ effect in $Sost^{-/-}$;$Lrp4^{KI/KI}$ mice. We therefore hypothesize that models with two inactivating $Lrp4^{KI}$ alleles rather activate bone remodeling, with a net gain in bone mass, whereas sclerostin deficiency has more robust anabolic effects on bone formation. Moreover, these effects of sclerostin and Lrp4 are stronger in female mice, contributing to a more severe phenotype than in males and more detectable phenotypic differences among different genotypes.

Keywords Lrp4 · Sost · Sclerostin · Sclerosteosis · High bone mass · RNA sequencing

Introduction

After decades of research, WNT signalling is considered a master regulator of skeletal homeostasis, and canonical or WNT/β-catenin signalling in particular an essential regulator of osteoblastic bone formation [1]. The latter has been supported by the identification of disease-causing variants in several components of the canonical WNT pathway in patients with high bone mass (HBM) disorders, also known as sclerosing bone dysplasias [2]. Causal variants have been identified in genes encoding extracellular regulators (*SOST*), co-receptors (*LRP4*, *LRP5*, *LRP6*) or intracellular regulators (*AMER1*, *CTNNB1*), contributing to unique HBM phenotypes, but generally sharing an increased activation of the canonical WNT pathway and induced osteoblastic bone formation [2].

Sclerosteosis is such a monogenic HBM disorder with an autosomal recessive inheritance pattern and marked by a generalized and progressive HBM, especially at the skull and tubular bones, macrocephaly and syndactyly [3]. Disease-causing variants have so far been identified in both *SOST* (MIM 269500) or *LRP4* (MIM 614305) [4–6]. These genes also reveal the affected underlying molecular mechanism, i.e. the interaction of the WNT antagonist sclerostin (encoded by *SOST*) with its receptor LRP4 (encoded by

✉ Wim Van Hul
wim.vanhul@uantwerpen.be

1 Centre for Medical Genetics, University and University Hospital of Antwerp, Antwerp, Belgium

2 Department of Human Genetics, KU Leuven, Louvain, Belgium

3 Department of Osteology and Biomechanics, University Medical Center Hamburg-Eppendorf, Hamburg, Germany

4 Diseases of Aging and Regenerative Medicine, Novartis Institutes for BioMedical Research, Basel, Switzerland

LRP4). Loss-of-function (LoF) variants in *SOST* that have been identified in sclerosteosis patients were reported to result in lower or even absent levels of sclerostin [7]. As an inhibitor of canonical WNT signaling, *SOST* LoF variants will therefore reduce the inhibition of the pathway, resulting in an increased osteoblastic bone formation, and a progressively dense skeleton. For *LRP4*, hypomorphic missense variants were initially only localised in the third β-propeller domain of the receptor [6, 8]. Deeper investigations revealed a sclerostin-interacting pocket in this region, and the mutations found by us and others (p.Arg1170Gln, p.Arg1170Trp and p.Trp1186Ser) were therefore proposed to specifically impair interaction with sclerostin and hence its inhibitory function on canonical WNT signaling [6, 8, 9]. Recently however, we reported that compound heterozygous variants in the 1st and 3rd β-propeller domain of LRP4 can also result in a sclerosteosis phenotype, broadening this receptor's mutational and mechanistic spectrum [10]. In addition, not only sclerostin but also other known modulators of canonical WNT signaling and bone metabolism e.g., Wise and Dickkopf1 (DKK1) are reported to interact with LRP4 [11, 12].

Both *SOST* and *LRP4* have been extensively studied in animal models to explore the underlying molecular and cellular mechanisms contributing to the related sclerosteosis phenotypes. *Sost* knockout ($Sost^{-/-}$) mice, for example, model the sclerosteosis-like HBM phenotype very well [13, 14]. On a cellular level, these mice have numerous enlarged osteoblasts, producing larger amounts of bone matrix, which led to the understanding that *Sost* deficiency has strong osteoanabolic effects. As for *Lrp4*, two specific knock-in models have been generated and studied by us ($Lrp4^{Arg1170Gln}$) [15] and others ($Lrp4^{Arg1170Trp}$) [16]. Also here, cellular studies have identified the osteoblast as the leading cell type during disease pathogenesis.

So far, findings in patients and animal models with *SOST*-related HBM phenotypes have inspired and motivated the pharmaceutical industry towards the development of monoclonal antibodies against sclerostin. Evidently, as reduced sclerostin levels have robust anabolic effects on osteoblastic bone formation, sclerostin has been an attractive therapeutic target for patients suffering from low bone mass and/or fragility fractures, such as osteoporosis. Currently, sclerostin neutralizing antibodies are perceived as one the most potent osteoporosis drugs [17]. As osteoporosis is a very common disorder affecting one in three women and one in five men above 55, this development has and will still have a large impact on our ageing society [18]. Accordingly, the 3rd β-propeller domain of Lrp4 has been suspected to provide an additional opportunity to augment osteoblastic canonical WNT signaling for therapeutic applications [19].

The primary goal of this study was to investigate a possible additive effect of the disease-causing p.Arg1170Trp variant in *LRP4* on *SOST* deficiency. For this purpose, we crossed *Sost* knockout ($Sost^{-/-}$) with *Lrp4* knock-in ($Lrp4^{KI/KI}$) mice carrying the inactivating p.Arg1170Trp variant, to generate $Sost^{-/-}$;$Lrp4^{KI/KI}$ mice for extensive phenotyping. Interestingly, we detected a milder HBM phenotype in female, not male, $Sost^{-/-}$;$Lrp4^{KI/KI}$ mice than in $Sost^{-/-}$ mice. Finally, RNA sequencing of $Lrp4^{KI/KI}$ primary osteoblasts was performed to provide us with unbiased molecular insights into the phenotypic features and differences we detected. By using this approach, we detected an unexpected upregulation of genes related to bone resorption and bone remodelling in $Lrp4^{KI/KI}$ primary osteoblasts.

Material and Methods

Animal Models

Two existing mutant ($Lrp4^{Arg1170Gln}$ and $Sost^{KO}$) mouse lines were used to create a novel compound mutant mouse line ($Sost^{KO}$;$Lrp4^{Arg1170Gln}$) for this study. Generation and genotyping of the *Sost* knockout ($Sost^{-/-}$) mouse model with a targeted disruption of the *Sost* coding region on a C57BL/6 J background was performed at Novartis and described elsewhere [13]. Standard PCR-based genotyping of $Sost^{KO}$ mice was done by using a mix of three primers; 5'-ACT CCA CAC GGT CTG GAA AGT GTT G-3'; 5'-TCC ACA ACC AGT CGG AGC TCA AGG-3' and 5'-GGG TGG GAT TAG ATA AAT GCC TGC TCT -3'. The $Lrp4^{Arg1170Gln}$ knock-in mouse model, hereafter referred to as $Lrp4^{KI}$ mice, on a C57BL/6N background was previously generated for us at Polygene AG (Rümlang Switzerland) [15]. Briefly, the LRP4 p.Arg1170 residue in humans corresponds to the Lrp4 p.Arg1170 in mice and the same G to A inactivating base pair change as found in sclerosteosis patients [9] was introduced in the mouse model, resulting in the loss of a *SmaI* restriction site that can be used for genotyping. Initially, heterozygous $Lrp4^{+/Arg1170Gln}$ were crossed with heterozygous $Sost^{\pm}$ mice to generate a novel compound mutant mouse line. These double mutant mice were then used for further breeding to generate mice with two mutant alleles of *Lrp4* and/or *Sost*.

Animal Husbandry and Experiments

All mice were held at the animal facility of the University of Antwerp and maintained on a 12 h light–dark cycle, with free access to regular chow and tap water. All animal experimental procedures were carried out in compliance with the ARRIVE guidelines [20] and were approved by the University of Antwerp Ethics Committee (reference number 2017-60). All following phenotypical analyses are performed on 5-month-old male ($n = 6$ per genotype)

and female mice ($n = 3$ per genotype). The genotypes investigated in this study are $Sost^{+/+};Lrp4^{+/+}$ (littermate controls), $Sost^{\pm};Lrp4^{+/KI}$, $Sost^{-/-};Lrp4^{+/+}$ ($Sost^{-/-}$) and $Sost^{-/-};Lrp4^{KI/KI}$.

Radiological Assessment

The skeletons were dissected and fixed in 3.7% PBS-buffered formaldehyde for 24 h after which they were transferred into 80% ethanol for an initial analysis by contact X-ray (35 kV, 2 s; Faxitron XRay Corp., USA). For µCT analysis the right femur of each mouse was dissected from the fixed mouse, before being placed into a radiotranslucent sample holder. Dehydration was prevented by filling the holder with PBS. µCT scanning and analysis was performed as previously described using a µCT 40 desktop cone-beam microCT (Scanco Medical, CHE) [21] according to standard guidelines [22].

Bone Histology

Vertebral bodies L1 to L4 and tibiae were dehydrated in ascending ethanol concentrations, before being embedded into methylmethacrylate. Sections of 4 µm thickness were cut in the sagittal plane (Microtec rotation microtome) and stained by von Kossa/van Gieson (for static histomorphometry) or toluidine blue (for cellular histomorphometry) as previously described [23]. To determine the bone formation rate, all mice were injected with calcein (30 mg/kg, i.p.) at 9 days and 2 days before euthanasia. Dynamic histomorphometry was performed on unstained 12 µm sections of the vertebral bodies. Static, cellular, and dynamic histomorphometry at trabecular bone surfaces was carried out according to the guidelines of the American Society for Bone and Mineral Research [24] using an OsteoMeasure system (Osteometrics Inc., Decatur, GA, USA) and Bioquant Osteo software (BIOQUANT Image Analysis Corp., Nashville, TN, USA) [21].

Cell Culture

Primary osteoblasts were isolated from the long bones of $Sost^{+/+};Lrp4^{+/+}$, $Sost^{+/+};Lrp4^{KI/KI}$ and $Sost^{-/-};Lrp4^{KI/KI}$ mice as described previously [25]. In brief, cleaned long bones were cut into small pieces and incubated with 2 mg/ml collagenase II (Sigma) solution for 2 h at 37 °C in a shaking water bath. Then, the bone fragments were washed and cultured in α-MEM containing 10% FCS, 100 U/ml penicillin, 100 µg/ml streptomycin, and 250 ng/ml amphotericin B in 25 cm^2 culture flasks. After confluence, bone fragments were removed, the confluent layers were trypsinized and the cells were replated in 25 cm^2 culture flasks until confluent.

Expression Analysis

RNA from primary osteoblasts was isolated using the ReliaPrep RNA Cell Miniprep System (Promega Corporation), and concentration and quality of total RNA were investigated using the Fragment Analyzer System (Agilent Technologies). For expression analysis, 1 µg of total RNA of high quality (RNA Quality Number (RQN) ≥ 7) from $Sost^{+/+};Lrp4^{+/+}$ ($n = 3$) and $Sost^{+/+};Lrp4^{KI/KI}$ mice ($n = 3$) was used for RNA sequencing (Eurofins Genomics). Here, the RNA Seq library was prepared using the TruSeq Stranded Total RNA Library Prep Kit (Illumina) and library validation was carried out using the Agilent 4200 TapeStation system (Agilent). RNA sequencing was carried out on an Illumina HiSeq platform and data analysis was performed using the mm10, v102 release ENSEMBL genome annotation. Differential gene expression was analyzed using DESeq2 [26]. The protein coding genes with an FDR-corrected P-values < 0.1 were considered significant. Gene set enrichment analysis was done with the package fGSEA in R using the Molecular Signatures Database (MSigDB) C5 biological processes and the C2 canonical pathways collection. For confirmation of differentially expressed genes with qRT-PCR, total RNA was reverse transcribed to cDNA using the Superscript III First Strand Synthesis System (Thermo Fisher Scientific) according to manufacturer's instructions. qPCR was performed using the qPCR Core kits for SYBR Green I, No ROX (Eurogentec). Each sample was analyzed in triplicate and *Gapdh* was included as reference gene (primer sequences available upon request). Relative quantification was performed according to the Livak method, where results are expressed in the linear form using the delta-delta comparative threshold cycle formula ($2^{-\Delta\Delta CT}$).

Biochemical Analysis

After sacrifice at 5 months of age, blood was drawn with cardiac puncture and serum was isolated and stored at −80 °C. Serum levels of the same mice were determined using ELISA of procollagen type-I C-terminal peptide (#SEA570Mu, PICP, Cloud-Clone Corp), collagen type 1 cross-linked C-telopeptide (CTX-1, #AC-06F1, Ratlaps EIA detecting CTX from ImmunoDiagnostic Systems), sclerostin (ab213889, Abcam), tartrate-resistant acid phosphatase (TRAP, LS-F54861, LifeSpanBiosciences Inc), receptor activator of nuclear factor kappa-B ligand (RANKL, MTR00, R&D Systems) and osteoprotegerin (OPG, M0P00, R&D Systems) according to the manufacturers' protocols.

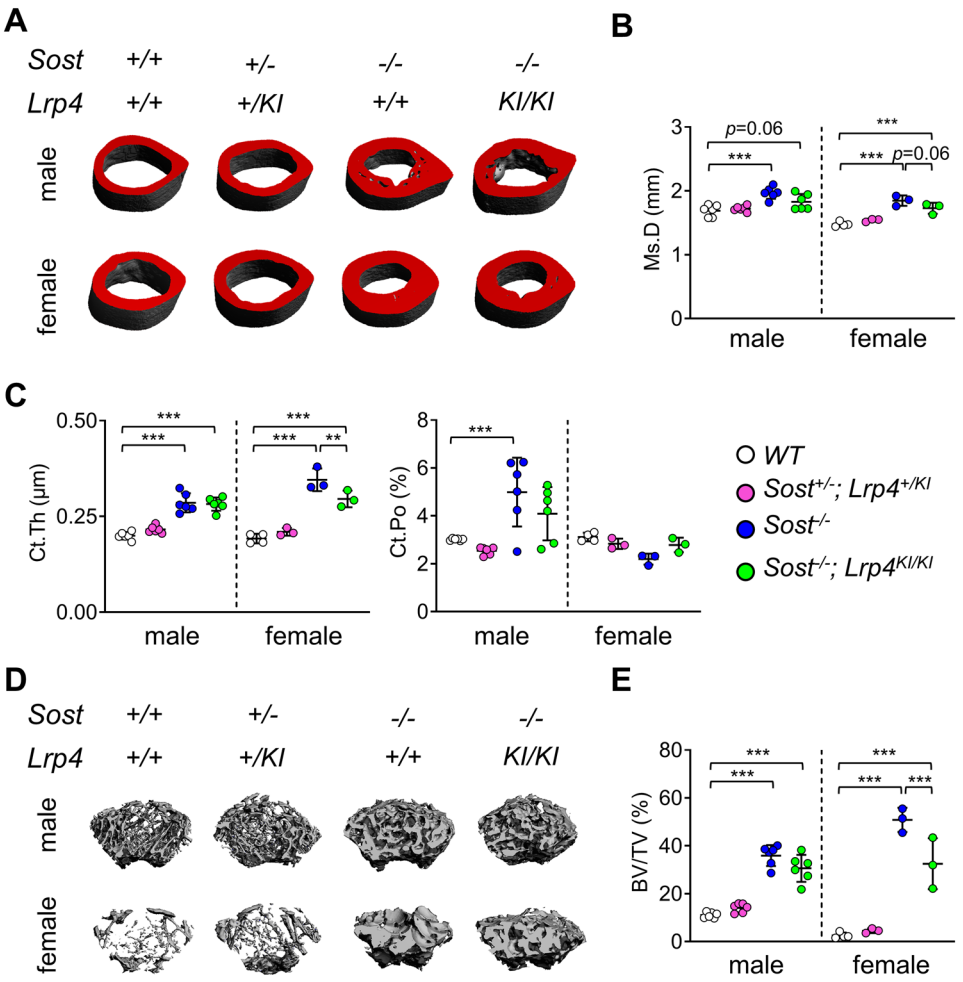

Fig. 1 µCT analysis of the femora demonstrates structural differences between female *Sost*$^{-/-}$ and *Sost*$^{-/-}$;*Lrp4*$^{KI/KI}$ mice. **A** Representative µCT images of the femoral cortical bone from 5-month-old male and female control, *Sost*$^{-/-}$, *Sost*$^{\pm}$;*Lrp4*$^{+/KI}$ and *Sost*$^{-/-}$;*Lrp4*$^{KI/KI}$ mice. **B** µCT-based quantification of the femoral Ms.D in control ($n=6$ male; $n=4$ female), *Sost*$^{\pm}$;*Lrp4*$^{+/KI}$ ($n=6$ male; $n=3$ female), *Sost*$^{-/-}$ ($n=6$ male; $n=3$ female) and *Sost*$^{-/-}$;*Lrp4*$^{KI/KI}$ mice ($n=6$ male; $n=3$ female). **C** µCT-based quantification of Ct.Th and Ct.Po in the femora of the same mice. **D** Representative µCT images of the femoral trabecular bone and **E** µCT-based quantification of the trabecular BV/TV in the same mice. Data are presented as individual data points with indication of mean ± SD, *p*-values obtained by one-way ANOVA with Šidák's multiple comparison test. *Ms.D* midshaft diameter; *Ct.Th* cortical thickness; *Ct.Po* cortical thickness; *BV/TV* bone volume per tissue volume

Statistical Analysis

Statistical analysis was performed by comparing multiple groups with different alleles of two independent genetic loci, with a one-way ANOVA with Šidák's multiple comparison test (GraphPad Software Inc., USA). All data are reported as the mean ± SD with additional points representing individual animals. A value of $P \leq 0.05$ was considered statistically significant.

Results

Additional Presence of *Lrp4*^{KI} Alleles Mitigate the *Sost*^{KO} High Bone Mass Phenotype

Five-month-old male and female *Sost*$^{+/+}$;*Lrp4*$^{+/+}$ (WT), *Sost*$^{\pm}$;*Lrp4*$^{+/KI}$, *Sost*$^{-/-}$;*Lrp4*$^{+/+}$ (*Sost*$^{-/-}$) and *Sost*$^{-/-}$;*Lrp4*$^{KI/KI}$ mice were collected for skeletal phenotyping. As a novel compound mutant mouse line, *Sost*$^{-/-}$;*Lrp4*$^{KI/KI}$ mice were viable and fertile.

We first performed µCT analysis of the femoral bones from male ($n=6$) and female mice ($n=3$) to analyse the structural properties of the cortical and trabecular bone compartments (Fig. 1). As for the cortical bone, we detected a larger midshaft diameter (Ms.D) in male and female *Sost*$^{-/-}$ femora and female *Sost*$^{-/-}$;*Lrp4*$^{KI/KI}$ mice, in comparison to controls (Fig. 1A–B). Cortical thickness (Ct.Th) was significantly higher in male and female *Sost*$^{-/-}$ and *Sost*$^{-/-}$;*Lrp4*$^{KI/KI}$ mice, compared to control mice. Interestingly, we detected a lower Ct.Th in female *Sost*$^{-/-}$;*Lrp4*$^{KI/KI}$ mice than in *Sost*$^{-/-}$ mice (Fig. 1C). Similarly, in the trabecular bone compartment, we observed a significant larger trabecular bone volume (BV/TV) in male and female *Sost*$^{-/-}$ and *Sost*$^{-/-}$;*Lrp4*$^{KI/KI}$ mice compared to wildtype controls, whereas BV/TV was significantly lower in female *Sost*$^{-/-}$;*Lrp4*$^{KI/KI}$ mice than in *Sost*$^{-/-}$ mice (Fig. 1D-E). Generally, we did not observe significant differences in the measured cortical or trabecular parameters in compound heterozygous mutant lines, i.e., male or female *Sost*$^{\pm}$;*Lrp4*$^{+/KI}$ mice, when compared to control mice (Fig. 1).

In parallel, structural properties of the trabecular bone were verified using Von Kossa/van Gieson

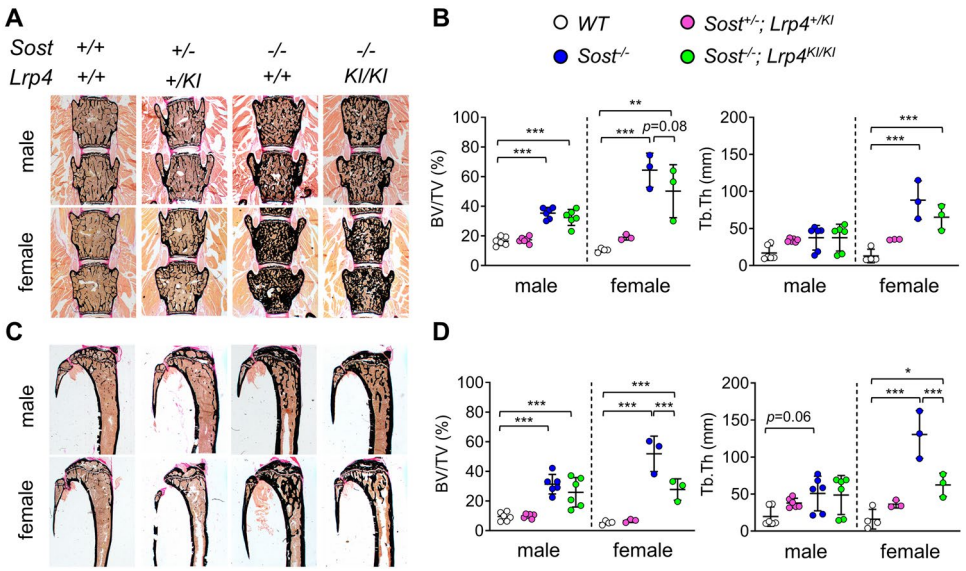

Fig. 2 Histomorphometry confirms structural differences between female *Sost*$^{-/-}$ and *Sost*$^{-/-}$;*Lrp4*$^{KI/KI}$ mice in the tibia, but not in spine. **A** Representative images after Von Kossa/van Gieson staining of lumbar spine sections of 5-month-old control, *Sost*$^{-/-}$, *Sost*$^{\pm}$;*Lrp4*$^{+/KI}$ and *Sost*$^{-/-}$;*Lrp4*$^{KI/KI}$ mice. **B** Quantification of the trabecular BV/TV and thickness in lumbar spine sections of control ($n=6$ male; $n=4$ female), *Sost*$^{\pm}$;*Lrp4*$^{+/KI}$ ($n=6$ male; $n=3$ female), *Sost*$^{-/-}$ ($n=6$ male; $n=3$ female) and *Sost*$^{-/-}$;*Lrp4*$^{KI/KI}$ mice ($n=6$ male; $n=3$ female). **C** Representative images of tibial sections after Von Kossa/van Gieson staining from 5-month old male and female control, *Sost*$^{-/-}$ and *Sost*$^{-/-}$;*Lrp4*$^{KI/KI}$ mice. **D** Quantification of the trabecular BV/TV and thickness in tibial sections of the same mice. Data are presented as individual data points with indication of mean ± SD, *p*-values obtained by one-way ANOVA with Šidák's multiple comparison test. *BV/TV* bone volume per tissue volume; *Tb.Th* trabecular thickness

histomorphometry on sections of the lumbar vertebral bodies (L1–L4) and tibiae of all mutant mice (Fig. 2). Both in the lumbar spine and tibiae, we detected a significant higher trabecular BV/TV in male and female *Sost*$^{-/-}$ and *Sost*$^{-/-}$;*Lrp4*$^{KI/KI}$ mice compared to controls, whereas an increase in the trabecular thickness (Tb.Th) was only present in females (Fig. 2). Interestingly, only in the tibiae but not in the vertebral bodies, BV/TV and Tb.Th values were significantly lower in female *Sost*$^{-/-}$;*Lrp4*$^{KI/KI}$ mice, in comparison to female *Sost*$^{-/-}$ mice (Fig. 2D). We again did not observe significant differences in any of the investigated trabecular parameters in double heterozygous mutant lines, compared to controls (Fig. 2).

Altogether, structural analysis of the long bones (femur, tibia) and lumbar spine, using µCT and histology, shows that *Sost*$^{-/-}$ and *Sost*$^{-/-}$;*Lrp4*$^{KI/KI}$ both present with a HBM phenotype in the cortical and trabecular compartments. This osteosclerotic phenotype was overall similar for male mice of both genotypes, but less severe in the long bones of female *Sost*$^{-/-}$;*Lrp4*$^{KI/KI}$ mice, than in *Sost*$^{-/-}$ mice.

Cellular Histomorphometry and Serum Biomarker Analysis of *Sost*$^{-/-}$ and *Sost*$^{-/-}$;*Lrp4*$^{KI/KI}$ Mice

Based on the structural differences that we observed between *Sost*$^{-/-}$ and *Sost*$^{-/-}$;*Lrp4*$^{KI/KI}$ mice, and lack of differences in the heterozygous mutant mouse lines, we focused on homozygous *Sost*$^{-/-}$ and *Sost*$^{-/-}$;*Lrp4*$^{KI/KI}$ mice for the remainder of our study.

Cellular histomorphometry was performed to detect potential cellular defects underlying the phenotypic differences that we described with µCT and histology. Quantification of the osteoblast number (N.Ob/B.Pm) and osteoblast-covered surface (Ob.S/BS) demonstrated no signficant differences for *Sost*$^{-/-}$ and *Sost*$^{-/-}$;*Lrp4*$^{KI/KI}$ mice, compared to WT controls and between both mutant models (Fig. 3A). There was however a trend towards a higher Ob.S/BS ($P=0.06$) in male *Sost*$^{-/-}$;*Lrp4*$^{KI/KI}$ mice, compared to WT mice (Fig. 3A). Osteoblast activity, which we quantified by using dynamic histomorphometry of the bone formation rate per bone surface area (BFR/BS), was significantly higher in male *Sost*$^{-/-}$ and *Sost*$^{-/-}$;*Lrp4*$^{KI/KI}$ mice, compared to controls (Fig. 3B). Similar tendencies were observed in female mice, however since non-evaluable samples reduced the group sizes, reliable statistical testing could not be performed. Histomorphometry of the osteoclasts indicated a lower osteoclast number (N.Oc/B.Pm)

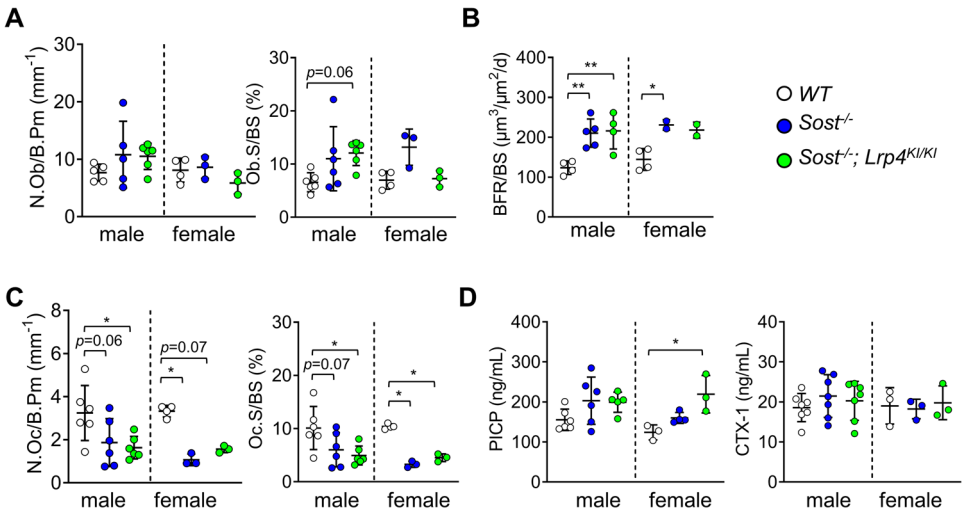

Fig. 3 Cellular and dynamic histomorphometry demonstrates higher bone formation rates and lower bone resorption parameters in *Sost*$^{-/-}$ and *Sost*$^{-/-}$;*Lrp4*$^{KI/KI}$ mice. **A** Histomorphometric quantification of N.Ob/B.Pm and Ob.S/BS in lumbar spine sections of 5-month-old control ($n=5$ male; $n=4$ female), *Sost*$^{-/-}$ ($n=6$ male; $n=3$ female) and *Sost*$^{-/-}$;*Lrp4*$^{KI/KI}$ mice ($n=6$ male; $n=3$ female). **B** Dynamic histomorphometry of the BFR/BS on lumbar spine sections of the same mice. **C** Histomorphometric quantification of the osteoclast number and covered surface in lumbar spine sections of the same mice. **D** Biochemical analysis of serum parameters for bone formation (PICP) and bone resorption (CTX-1) the same mice. Data are presented as individual data points with indication of mean ± SD, *p*-values obtained by one-way ANOVA with Šidák's multiple comparison test. *BV/TV* bone volume per tissue volume; *Tb.Th* trabecular thickness. *N.Ob/B.Pm* number of osteoblasts per bone perimeter; *Ob.S/BS* osteoblast surface per bone surface; *BFR/BS* bone formation rate per bone surface; *N.Oc/B.Pm* number of osteoclasts per bone perimeter; *Oc.S/BS* osteoclast surface per bone surface; *PICP* procollagen type-I C-terminal peptide; *CTX-1* collagen type 1 cross-linked C-telopeptide

and osteoclast-covered surface (Oc.S/BS) in *Sost*$^{-/-}$ and *Sost*$^{-/-}$;*Lrp4*$^{KI/KI}$ mice, compared to WT mice (Fig. 3C). We did not observe significant differences between *Sost*$^{-/-}$ and *Sost*$^{-/-}$;*Lrp4*$^{KI/KI}$ mice. In parallel, we quantified bone formation (PICP) and resorption (CTX-1) markers in the serum of 5-month-old controls, *Sost*$^{-/-}$ and *Sost*$^{-/-}$;*Lrp4*$^{KI/KI}$ mice by using ELISA. These biochemical analyses revealed a significant higher level of PICP in female *Sost*$^{-/-}$;*Lrp4*$^{KI/KI}$ mice, in comparison to controls (Fig. 3D). Again, no differences between serum markers of *Sost*$^{-/-}$ and *Sost*$^{-/-}$;*Lrp4*$^{KI/KI}$ mice of both genders were detected.

Our cellular and dynamic analyses shows an induction of osteoblast activity and a reduction in osteoclast-related parameters in *Sost*$^{-/-}$ and *Sost*$^{-/-}$;*Lrp4*$^{KI/KI}$ mice, whereas either mild or no differences were found in bone formation or resorption serum markers in these mice.

Transcriptome-Wide Expression Analysis of *Lrp4*$^{KI/KI}$ Osteoblasts Reveals Upregulation of Genes Related to Bone Resorption and Remodeling

Skeletal phenotyping of *Sost*$^{-/-}$ and *Sost*$^{-/-}$;*Lrp4*$^{KI/KI}$ demonstrated that the additional presence of two *Lrp4*^{KI} alleles affects the integrity of the *Sost*$^{-/-}$ HBM phenotype, especially in female mice. We could however not explain these phenotypic differences by standard cellular and biochemical analyses (Fig. 3).

To improve our understanding of the effect of *Lrp4*^{KI} alleles on a molecular level, we next performed bulk RNA sequencing on three independent sets of primary long bone osteoblasts of *Lrp4*$^{+/+}$ and *Lrp4*$^{KI/KI}$ mice. Here, looking at the adjusted P-values, only 14 genes showed a significant differential expression in *Lrp4*$^{KI/KI}$ primary osteoblasts, in comparison to *Lrp4*$^{+/+}$ osteoblasts (Fig. 4A–B). Most of these genes, unexpectedly, seemed to be related to osteoclast biology at first sight, e.g. *Mmp9*, *Acp5* (also known as *Trap*), *Dcstamp*, *Oscar* and *Tnfsf11* (also known as *Rankl*) (Fig. 4B). In line with this, gene ontology (GO) pathway analysis demonstrated a significant enrichment of genes related to osteoclast differentiation or activity (Fig. 4C). 'Positive regulation of osteoclast differentiation' (GO:0045672) was the most enriched biological process in *Lrp4*$^{KI/KI}$ osteoblasts, with a normalized enrichment score (NES) of 2.22. Other significantly enriched biological processes related to bone resorption were 'osteoclast development' (GO:0036035; NES 2.12), 'bone resorption' (GO:0045453; NES 2.07), 'regulation of osteoclast development' (GO:2001204; NES 2.04), 'keratan sulfate catabolic process' (GO:0042340; NES 1.94), 'multinuclear osteoclast differentiation' (GO:0072674; NES 1.89) and 'positive regulation of osteoclast development' (GO:2001206; NES 1.85). On the other hand, biological processes related to bone modelling ('skeletal system development'; GO:0001501; NES 1.85) or

bone remodeling ('positive regulation of tissue remodeling'; GO:0034105; NES 2.19 and 'tissue remodeling'; GO:0048771; NES 1.98) were significantly enriched in $Lrp4^{KI/KI}$ osteoblasts (Fig. 4C). Remarkably, no biological processes related to osteoblast differentiation, functioning or general bone formation were detected in $Lrp4^{KI/KI}$ osteoblasts through GO analysis, despite the HBM phenotype of $Lrp4^{KI/KI}$ mice that we had described previously [15].

Based on our RNA sequencing data and GO pathway analysis, we selected *Mmp9* (encoding matrix metalloprotease 9), *Acp5* (encoding acid phosphatase 5 or tartrate-resistant acid phosphatase (TRAP)) and *Tnfsf11* (encoding the receptor activator of nuclear factor kappa-B ligand (Rankl)) for confirmation with qRT-PCR in $Lrp4^{KI/KI}$ osteoblasts and verification in $Sost^{-/-}$ and $Sost^{-/-}$; $Lrp4^{KI/KI}$ osteoblasts. For *Mmp9*, *Acp5* and *Tnfsf11*, we confirmed upregulation of these genes in $Lrp4^{KI/KI}$ primary osteoblasts, in comparison to WT osteoblasts, although this was not reaching the significance threshold for *Mmp9* ($P = 0.18$) and *Tnfsf11* ($P = 0.08$) (Fig. 4D). For *Acp5*, on the other hand, we detected a significant 40-fold higher expression in $Lrp4^{KI/KI}$ osteoblasts ($P < 0.01$) than in WT osteoblasts. In $Sost^{-/-}$;$Lrp4^{KI/KI}$ osteoblasts, *Acp5* expression was still tenfold higher than in WT osteoblasts, and significantly lower in comparison to $Lrp4^{KI/KI}$ osteoblasts. Although not significant due to large sample variability, it was remarkable to note that *Mmp9* expression was on average 250-fold higher in $Lrp4^{KI/KI}$ osteoblasts and 100-fold higher in $Sost^{-/-}$;$Lrp4^{KI/KI}$ osteoblasts, compared to controls. In $Sost^{-/-}$ osteoblasts, we detected no differences in the expression of *Mmp9* or *Acp5*, in comparison to WT osteoblasts, whereas *Tnfsf11* expression was nearly reduced by half ($P < 0.05$) (Fig. 4D). Finally, *Tnfsf11* expression was also lower in $Sost^{-/-}$; $Lrp4^{KI/KI}$ primary osteoblasts, in comparison to both $Lrp4^{KI/KI}$ ($P = 0.06$) and WT osteoblasts ($P < 0.05$) (Fig. 4D).

Next, we decided to quantify the levels of TRAP (encoded by *Acp5*), RANKL and osteoprotegerin (OPG) in serum of 5-month-old control, $Lrp4^{KI/KI}$, $Sost^{-/-}$ and $Sost^{-/-}$;$Lrp4^{KI/KI}$ mice by using ELISA. In these mice, we could not detect any differences in the individual serum levels of RANKL or OPG (Fig. 5A). We then calculated the individual RANKL/OPG ratios in these mice, detecting a higher RANKL/OPG ratio in $Sost^{-/-}$ mice, in comparison to either $Lrp4^{KI/KI}$ or $Sost^{-/-}$; $Lrp4^{KI/KI}$ mice (Fig. 5B). In contrast to our transcriptomic and qRT-PCR data, TRAP serum levels were not significantly higher in $Lrp4^{KI/KI}$ mice, although a higher trend could be noted, compared to controls. Interestingly, significantly lower TRAP levels were detected in male and female $Sost^{-/-}$ and $Sost^{-/-}$; $Lrp4^{KI/KI}$ mice, when compared to $Lrp4^{KI/KI}$ mice (Fig. 5C), supporting our osteoclast histomorphometry data (Fig. 3C).

Overall, our transcriptomic and biochemical analyses of primary osteoblasts indicate that the presence of the *Lrp4* p.Arg1170Gln mutation results in the upregulation of genes related to bone resorption and remodeling. These markers are no longer or markedly less induced in osteoblasts or serum of $Sost^{-/-}$ and $Sost^{-/-}$;$Lrp4^{KI/KI}$ mice, indicating a dominant countereffect by *Sost* deficiency.

Discussion

In the current study, we have generated a novel $Sost^{-/-}$;$Lrp4^{KI/KI}$ mouse line, and compared it to the phenotype of $Sost^{-/-}$ mice to evaluate synergistic effects of the inactivating p.Arg1170Trp mutation in *Lrp4* on *Sost* deficiency. This compound mutant mouse model was created by crossing $Sost^{-/-}$ with $Lrp4^{KI/KI}$ mice, of which the latter was described previously by us [15]. First of all, phenotypic comparison of $Sost^{-/-}$ [13] and $Lrp4^{KI/KI}$ mice shows that both single mutant models present with a sclerosteosis-like phenotype, although *Sost*-related HBM is more severe. Based on the mutations initially found in patients with *LRP4*-related sclerosteosis, it was thought that the 3rd β-propeller domain of LRP4 was the sclerostin-interacting pocket, explaining the significant phenotypic overlap between *SOST*- and *LRP4*-related sclerosteosis [6, 8, 9]. Recently, however, we have shown that compound heterozygous mutations in the 1st and 3rd β-propeller domain of *LRP4* can also cause sclerosteosis [10]. This indicates that some residual sclerostin binding and inhibitory actions might still be present in $Lrp4^{KI/KI}$ mice carrying a homozygous mutation in the 3rd β-propeller, providing a possible explanation why their phenotype is less severe than in $Sost^{-/-}$ mice. We hypothesized that $Sost^{-/-}$;$Lrp4^{KI/KI}$ mice might have a more severe sclerosteosis phenotype than single mutant mice. A double mutant background would, in that case, further impair the inhibitory effect of sclerostin-Lrp4 on canonical WNT signaling and impair the binding of other WNT inhibitors (e.g., Dickkopf1, Wise) that also bind Lrp4's extracellular domain [11, 27] and might still have compensatory effects in $Sost^{-/-}$ mice. Unexpectedly, however, skeletal phenotyping of male $Sost^{-/-}$ and $Sost^{-/-}$;$Lrp4^{KI/KI}$ mice showed no differences, whereas female $Sost^{-/-}$;$Lrp4^{KI/KI}$ mice had a HBM phenotype that was less severe than that of $Sost^{-/-}$ mice. This effect appeared to be specific for the appendicular skeleton as differences were noticeable in the cortical and trabecular bone compartment of the long bones, and not in the spine, of female $Sost^{-/-}$;$Lrp4^{KI/KI}$ mice.

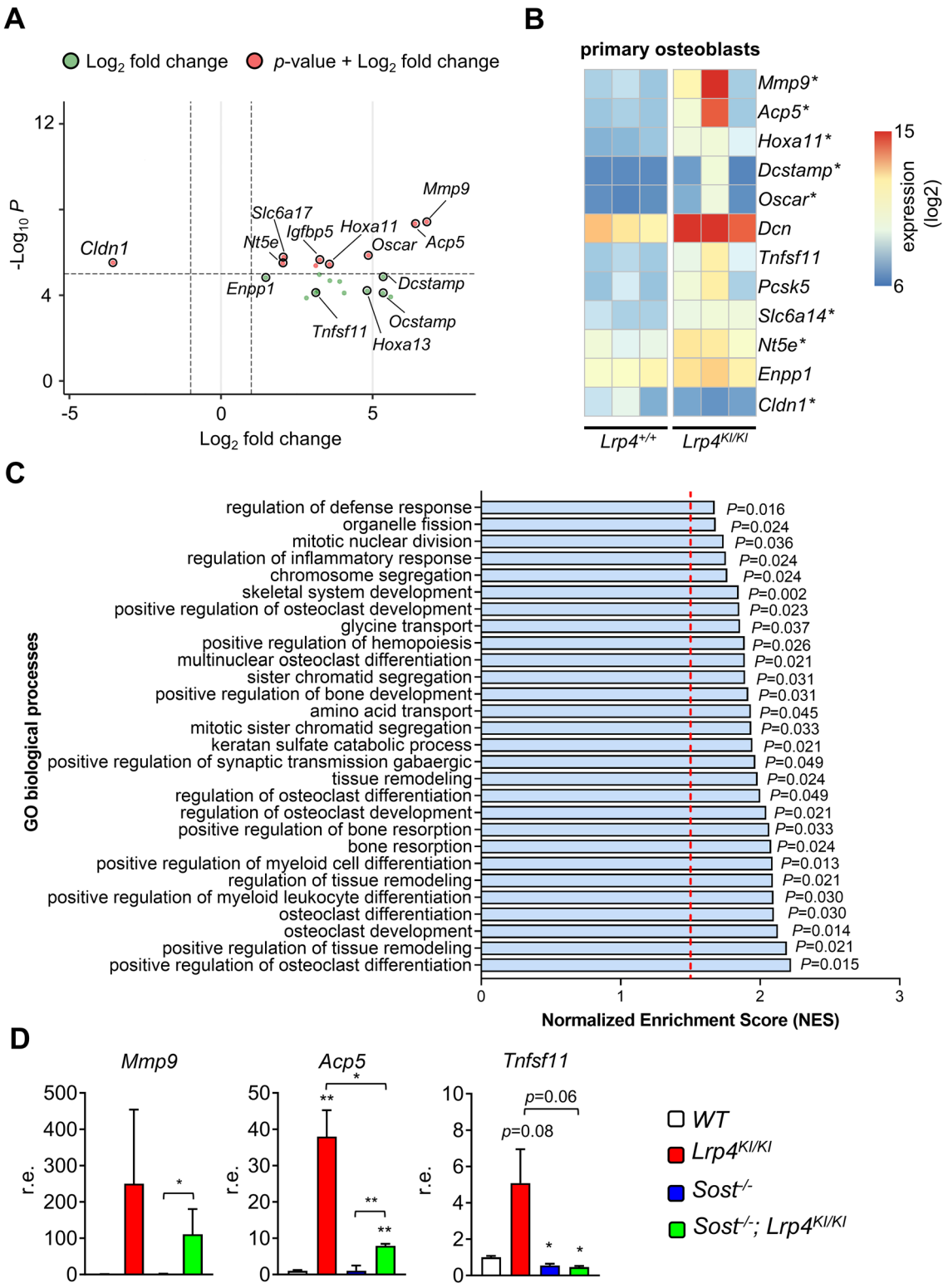

The HBM phenotype of male $Sost^{-/-}$;$Lrp4^{KI/KI}$ mice was similar to that of male $Sost^{-/-}$ mice, and more severe than what we previously observed in $Lrp4^{KI/KI}$ mice [15]. This finding is most likely due to a dominant and robust osteoanabolic effect of sclerostin deficiency, which is reflected by higher bone formation rates. We can conceptually compare these findings with a previous study, where wildtype and *Lrp4* p.Arg1170Trp knock-in mice were treated with a sclerostin neutralizing monoclonal antibody (Scl-mAb) [16]. Bullock and colleagues observed

◂**Fig. 4** Transcriptome analysis of $Lrp4^{KI/KI}$ primary osteoblasts demonstrates upregulation of genes involved in bone resorption and bone remodeling. **A** Volcano plot of all the differentially expressed genes in three independent sets of $Lrp4^{+/+}$ versus $Lrp4^{KI/KI}$ primary osteoblasts. **B** Heat map showing the expression of a selection of differentially expressed genes in $Lrp4^{KI/KI}$ primary osteoblasts, in comparison to $Lrp4^{+/+}$ primary osteoblasts. An asterisk indicates a significant differential expression. **C** Gene Ontology (GO) enrichment analysis of genes differentially expressed in $Lrp4^{KI/KI}$ primary osteoblasts, compared to $Lrp4^{+/+}$ primary osteoblasts. The values behind the bar graph are adjusted *p*-values based on the hypergeometric test. The vertical red dotted line indicates the threshold value for the normilized enrichment score (NES > + 1.5). **D** qRT-PCR analysis of *Mmp9*, *Acp5* and *Tnfsf11* in primary osteoblasts from wildtype, $Lrp4^{KI/KI}$, $Sost^{-/-}$ and $Sost^{-/-};Lrp4^{KI/KI}$ mice. Data are presented as bar graphs with mean ± SD, *p*-values obtained by one-way ANOVA with Šidák's multiple comparison test

blunted effects of the Scl-mAb induced gain in BMD and µCT-derived parameters in $Lrp4^{KI/KI}$ mice, which was about half of that exhibited by wildtype mice treated with Scl-mAb. They concluded that the strong anabolic effects of Scl-mAb were compromised or absent in $Lrp4^{KI/KI}$ mice, likely due to the mutation having similar functional (i.e., redundant) effects as sclerostin neutralization. This is similar to what we have observed in male wildtype, $Sost^{-/-}$ and $Sost^{-/-};Lrp4^{KI/KI}$ mice, although our findings in female mice were surprisingly different.

Female mice consistently exhibited a more severe skeletal phenotype than males in our study, especially in the trabecular bone compartment (spine and long bones). Furthermore, long bones of female $Sost^{-/-};Lrp4^{KI/KI}$ mice were less severely and robustly affected by HBM than long bones from $Sost^{-/-}$ females. These findings indicate gender-specific effects on the establishment of *Sost*- and/or *Sost;Lrp4*-related HBM phenotypes, especially in the long bones and trabecular bone compartment. Trabecular bone in particular is tightly regulated by bone turnover and mechanical loading is an anabolic trigger for this process, especially in the long bones [28, 29]. Our data therefore suggest that female mice are more sensitive for the effects of sclerostin and Lrp4 on this balance between osteoblasts and osteoclasts. For patients with *SOST*- or *LRP4*-related forms of sclerosteosis, it is more difficult to draw conclusions regarding gender-related differences, due to the low numbers of patients and phenotypic variability.

On a cellular level, osteoblasts have consistently been identified as the main cell type driving the development of $Sost^{-/-}$ or $Lrp4^{KI/KI}$ phenotypes, characterized by a greater anabolic capacity of individual osteoblasts (bone formation rates). As for bone resorption, osteoclast-related parameters were significantly lower in $Sost^{-/-}$ and $Sost^{-/-};Lrp4^{KI/KI}$ mice, which was previously reported in $Sost^{-/-}$ mice but not in our $Lrp4^{KI/KI}$ mice [13, 15]. In contrast, we previously noticed slightly but not significantly elevated values for osteoclastic parameters in our $Lrp4^{KI/KI}$ mice [15]. For the *Lrp4* knock-in mice carrying the p.Arg1170Trp variant, osteoclast histomorphometry data were not included [16]. Overall, it is evident that sclerostin deficiency has dominant osteoanabolic and anti-resorptive effects in male and female $Sost^{-/-}$ and $Sost^{-/-};Lrp4^{KI/KI}$ mice. Also in postmenopausal women, monoclonal antibodies that bind and inhibit sclerostin (e.g., Romosozumab), have also been reported to have a dual effect of increasing bone formation and decreasing bone resorption [17, 30, 31]. Based on the data in this study, however, the robust net gain in bone mass due to sclerostin deficiency seems partially compromised in female $Sost^{-/-};Lrp4^{KI/KI}$ mice, due to the presence of $Lrp4^{KI/KI}$ alleles.

Contrary to our expectations, an unbiased whole-transcriptome analysis of $Lrp4^{KI/KI}$ primary osteoblasts revealed an upregulation of genes related to osteoclast activity and differentiation and bone remodeling. While it is unclear why no genes related to osteoblastic bone formation came out of this analysis, it may offer some molecular insights on the phenotypic features and differences observed in $Lrp4^{KI/KI}$, $Sost^{-/-}$ and $Sost^{-/-};Lrp4^{KI/KI}$ mice. Previous studies have indicated that the function of Lrp4 in osteoblasts is to suppress bone formation and promote osteoclastogenesis and bone resorption, through inhibition of canonical WNT signaling [12]. Importantly, however, these insights were obtained from experiments using conditional *Lrp4* knockout mice. Based on our phenotypic, cellular and molecular data, we assume that the p.Arg1170Gln variant in the 3rd β-propeller of Lrp4 has unique effects on bone turnover, with a net gain in bone mass as phenotypic outcome. Alternatively, it might also be that primary osteoblasts from $Lrp4^{KI/KI}$ mice do not have cell-autonomous defects on their differentiation or function, which could also (partially) explain why no genes related to these processes were differentially expressed.

In conclusion, we did not observe an additive effect of the disease-causing p.Arg1170Trp variant in *Lrp4* on *Sost* deficiency. In fact, surprisingly, the *Lrp4* variant partially mitigated the effect of the *SOST* deficiency specifically in long bones of female mice. Molecular analysis of $Lrp4^{KI/KI}$ osteoblasts revealed an unexpected increase in the expression of genes related to bone resorption and remodeling. We therefore hypothesize that mouse models with two $Lrp4^{KI}$ alleles rather activate bone remodeling, with a net gain in bone mass, whereas sclerostin deficiency has more robust anabolic effects on bone formation. Future studies, studying the molecular background of *Sost*-deficient osteoblasts/osteocytes or *Lrp4*-mutant osteoblasts, with a mutation outside of the 3rd β-propeller domain, could further improve our understanding of the pathogenesis of their associated high bone mass phenotypes.

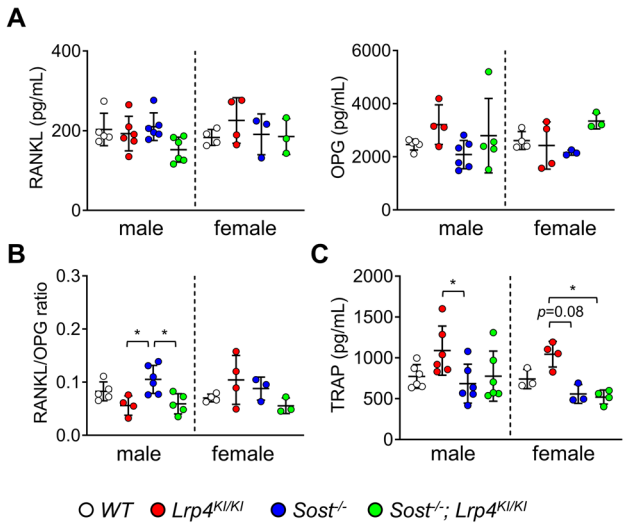

Fig. 5 Biochemical verification of RANKL, OPG and TRAP in serum of single and double mutant mouse models. **A** ELISA-based quantification of RANKL and OPG levels in the serum of 5-month-old control ($n=5$ male; $n=4$ female), $Lrp4^{KI/KI}$ ($n=4$–6 male; $n=4$ female), $Sost^{-/-}$ ($n=4$–6 male; $n=4$ female) and $Sost^{-/-}$;$Lrp4^{KI/KI}$ mice ($n=6$ male; $n=3$ female). **B** Calculated RANKL/OPG ratios from these mice based on their individual RANKL and OPG serum levels. **C** ELISA-based quantification of TRAP levels in the serum of these mice. Data are presented as individual data points with indication of mean ± SD, *p*-values obtained by one-way ANOVA with Šidák's multiple comparison test

Author Contributions Conceptualization, GH, EB and WVH; Data curation, GH and EB; Formal analysis, GH, EB, LM and TAY; and Methodology, GH, EB, LM, TAY and ES; Supervision, WVH; Validation, GH, EB and LM; Writing—original draft, GH and WVH; Writing—review & editing, GH, EB, LM, TAY, ES, MK, IK, GM, TS and WVH. All authors listed have made a substantial, direct, and intellectual contribution to the work and have approved it for publication. All authors have read and agreed to the published version of the manuscript.

Funding This research was funded by grants of the Fund for Scientific Research Flanders (FWO grant G031915N), a personal grant to EB (FWO personal grant 12A3814N), a research grant of the University of Antwerp (Methusalem—OEC grant—"GENOMED"; FFB190208) and the European Community's Seventh Framework Programme (FP7/2007-2013) under grant agreement no. 602300 (SYBIL).

Declarations

Conflict of interests GH, EB, LM, TAY, ES, GM, TS and WVH declare that they have no conflict of interest. MK and IK are employees of Novartis Institutes for BioMedical Research.

Compliance with Ethical Standards All animal experimental procedures were carried out in compliance with the ARRIVE guidelines and European Commission Council Directive 2010/63/EU on protecting animals for scientific purposes and ethical approval for all procedures was obtained by the University of Antwerp Ethics Committee (Reference Number 2017-60).

Human and Animal Rights All animal experimental procedures were carried out in compliance with the ARRIVE guidelines and were approved by the University of Antwerp Ethics Committee (reference number 2017-60).

Informed Consent No informed consent statement.

References

1. Huybrechts Y, Mortier G, Boudin E, Van Hul W (2020) WNT signaling and bone: lessons from skeletal dysplasias and disorders. Front Endocrinol (Lausanne) 11:165
2. Bergen DJM, Maurizi A, Formosa MM, McDonald GLK, El-Gazzar A, Hassan N, Brandi ML, Riancho JA, Rivadeneira F, Ntzani E, Duncan EL, Gregson CL, Kiel DP, Zillikens MC, Sangiorgi L, Hogler W, Duran I, Makitie O, Van Hul W, Hendrickx G (2023) High bone mass disorders: new insights from connecting the clinic and the bench. J Bone Miner Res 38:229–247
3. Hamersma H, Gardner J, Beighton P (2003) The natural history of sclerosteosis. Clin Genet 63:192–197
4. Balemans W, Ebeling M, Patel N, Van Hul E, Olson P, Dioszegi M, Lacza C, Wuyts W, Van Den Ende J, Willems P, Paes-Alves AF, Hill S, Bueno M, Ramos FJ, Tacconi P, Dikkers FG, Stratakis C, Lindpaintner K, Vickery B, Foernzler D, Van Hul W (2001) Increased bone density in sclerosteosis is due to the deficiency of a novel secreted protein (SOST). Hum Mol Genet 10:537–543
5. Brunkow ME, Gardner JC, Van Ness J, Paeper BW, Kovacevich BR, Proll S, Skonier JE, Zhao L, Sabo PJ, Fu Y, Alisch RS, Gillett L, Colbert T, Tacconi P, Galas D, Hamersma H, Beighton P, Mulligan J (2001) Bone dysplasia sclerosteosis results from loss of the SOST gene product, a novel cystine knot-containing protein. Am J Hum Genet 68:577–589
6. Leupin O, Piters E, Halleux C, Hu S, Kramer I, Morvan F, Bouwmeester T, Schirle M, Bueno-Lozano M, Fuentes FJ, Itin PH, Boudin E, de Freitas F, Jennes K, Brannetti B, Charara N, Ebersbach H, Geisse S, Lu CX, Bauer A, Van Hul W, Kneissel M (2011) Bone overgrowth-associated mutations in the LRP4 gene impair sclerostin facilitator function. J Biol Chem 286:19489–19500
7. van Lierop AH, Hamdy NA, Hamersma H, van Bezooijen RL, Power J, Loveridge N, Papapoulos SE (2011) Patients with sclerosteosis and disease carriers: human models of the effect of sclerostin on bone turnover. J Bone Miner Res 26:2804–2811
8. Ohkawara B, Cabrera-Serrano M, Nakata T, Milone M, Asai N, Ito K, Ito M, Masuda A, Ito Y, Engel AG, Ohno K (2014) LRP4 third beta-propeller domain mutations cause novel congenital myasthenia by compromising agrin-mediated MuSK signaling in a position-specific manner. Hum Mol Genet 23:1856–1868
9. Fijalkowski I, Geets E, Steenackers E, Van Hoof V, Ramos FJ, Mortier G, Fortuna AM, Van Hul W, Boudin E (2016) A novel domain-specific mutation in a sclerosteosis patient suggests a role of LRP4 as an anchor for sclerostin in human bone. J Bone Miner Res 31:874–881
10. Huybrechts Y, Boudin E, Hendrickx G, Steenackers E, Hamdy N, Mortier G, Martinez Diaz-Guerra G, Bracamonte MS, Appelman-Dijkstra NM, Van Hul W (2022) Identification of compound heterozygous variants in LRP4 demonstrates that a pathogenic variant

outside the third beta-propeller domain can cause sclerosteosis. Genes (Basel) 13:80
11. Choi HY, Dieckmann M, Herz J, Niemeier A (2009) Lrp4, a novel receptor for Dickkopf 1 and sclerostin, is expressed by osteoblasts and regulates bone growth and turnover in vivo. PLoS ONE 4:e7930
12. Xiong L, Jung JU, Wu H, Xia WF, Pan JX, Shen C, Mei L, Xiong WC (2015) Lrp4 in osteoblasts suppresses bone formation and promotes osteoclastogenesis and bone resorption. Proc Natl Acad Sci USA 112:3487–3492
13. Kramer I, Loots GG, Studer A, Keller H, Kneissel M (2010) Parathyroid hormone (PTH)-induced bone gain is blunted in SOST overexpressing and deficient mice. J Bone Miner Res 25:178–189
14. Li X, Ominsky MS, Niu QT, Sun N, Daugherty B, D'Agostin D, Kurahara C, Gao Y, Cao J, Gong J, Asuncion F, Barrero M, Warmington K, Dwyer D, Stolina M, Morony S, Sarosi I, Kostenuik PJ, Lacey DL, Simonet WS, Ke HZ, Paszty C (2008) Targeted deletion of the sclerostin gene in mice results in increased bone formation and bone strength. J Bone Miner Res 23:860–869
15. Boudin E, Yorgan T, Fijalkowski I, Sonntag S, Steenackers E, Hendrickx G, Peeters S, De Mare A, Vervaet B, Verhulst A, Mortier G, D'Haese P, Schinke T, Van Hul W (2017) The Lrp4R1170Q homozygous knock-in mouse recapitulates the bone phenotype of sclerosteosis in humans. J Bone Miner Res 32:1739–1749
16. Bullock WA, Hoggatt AM, Horan DJ, Elmendorf AJ, Sato AY, Bellido T, Loots GG, Pavalko FM, Robling AG (2019) Lrp4 mediates bone homeostasis and mechanotransduction through interaction with sclerostin in vivo. iScience 20:205–215
17. Cosman F, Crittenden DB, Adachi JD, Binkley N, Czerwinski E, Ferrari S, Hofbauer LC, Lau E, Lewiecki EM, Miyauchi A, Zerbini CA, Milmont CE, Chen L, Maddox J, Meisner PD, Libanati C, Grauer A (2016) Romosozumab treatment in postmenopausal women with osteoporosis. N Engl J Med 375:1532–1543
18. Hendrickx G, Boudin E, Van Hul W (2015) A look behind the scenes: the risk and pathogenesis of primary osteoporosis. Nat Rev Rheumatol 11:462–474
19. Chang MK, Kramer I, Huber T, Kinzel B, Guth-Gundel S, Leupin O, Kneissel M (2014) Disruption of Lrp4 function by genetic deletion or pharmacological blockade increases bone mass and serum sclerostin levels. Proc Natl Acad Sci USA 111:E5187-5195
20. Percie du Sert N, Ahluwalia A, Alam S, Avey MT, Baker M, Browne WJ, Clark A, Cuthill IC, Dirnagl U, Emerson M, Garner P, Holgate ST, Howells DW, Hurst V, Karp NA, Lazic SE, Lidster K, MacCallum CJ, Macleod M, Pearl EJ, Petersen OH, Rawle F, Reynolds P, Rooney K, Sena ES, Silberberg SD, Steckler T, Wurbel H (2020) Reporting animal research: explanation and elaboration for the ARRIVE guidelines 2.0. PLoS Biol 18:e3000411
21. Yorgan TA, Peters S, Jeschke A, Benisch P, Jakob F, Amling M, Schinke T (2015) The anti-osteoanabolic function of sclerostin is blunted in mice carrying a high bone mass mutation of Lrp5. J Bone Miner Res 30:1175–1183
22. Bouxsein ML, Boyd SK, Christiansen BA, Guldberg RE, Jepsen KJ, Muller R (2010) Guidelines for assessment of bone microstructure in rodents using micro-computed tomography. J Bone Miner Res 25:1468–1486
23. Albers J, Keller J, Baranowsky A, Beil FT, Catala-Lehnen P, Schulze J, Amling M, Schinke T (2013) Canonical Wnt signaling inhibits osteoclastogenesis independent of osteoprotegerin. J Cell Biol 200:537–549
24. Parfitt AM, Drezner MK, Glorieux FH, Kanis JA, Malluche H, Meunier PJ, Ott SM, Recker RR (1987) Bone histomorphometry: standardization of nomenclature, symbols, and units. Report of the ASBMR histomorphometry nomenclature committee. J Bone Miner Res 2:595–610
25. Hendrickx G, Borra VM, Steenackers E, Yorgan TA, Hermans C, Boudin E, Waterval JJ, Jansen IDC, Aydemir TB, Kamerling N, Behets GJ, Plumeyer C, D'Haese PC, Busse B, Everts V, Lammens M, Mortier G, Cousins RJ, Schinke T, Stokroos RJ, Manni JJ, Van Hul W (2018) Conditional mouse models support the role of SLC39A14 (ZIP14) in hyperostosis cranialis interna and in bone homeostasis. PLoS Genet 14:e1007321
26. Love MI, Huber W, Anders S (2014) Moderated estimation of fold change and dispersion for RNA-seq data with DESeq2. Genome Biol 15:550
27. Ohazama A, Johnson EB, Ota MS, Choi HY, Porntaveetus T, Oommen S, Itoh N, Eto K, Gritli-Linde A, Herz J, Sharpe PT (2008) Lrp4 modulates extracellular integration of cell signaling pathways in development. PLoS ONE 3:e4092
28. Ozcivici E, Luu YK, Adler B, Qin YX, Rubin J, Judex S, Rubin CT (2010) Mechanical signals as anabolic agents in bone. Nat Rev Rheumatol 6:50–59
29. Papachroni KK, Karatzas DN, Papavassiliou KA, Basdra EK, Papavassiliou AG (2009) Mechanotransduction in osteoblast regulation and bone disease. Trends Mol Med 15:208–216
30. McClung MR, Grauer A, Boonen S, Bolognese MA, Brown JP, Diez-Perez A, Langdahl BL, Reginster JY, Zanchetta JR, Wasserman SM, Katz L, Maddox J, Yang YC, Libanati C, Bone HG (2014) Romosozumab in postmenopausal women with low bone mineral density. N Engl J Med 370:412–420
31. Padhi D, Jang G, Stouch B, Fang L, Posvar E (2011) Single-dose, placebo-controlled, randomized study of AMG 785, a sclerostin monoclonal antibody. J Bone Miner Res 26:19–26